Communication

Electric Field Integral Equation-Based Synthesis of Elliptical-Domain Metasurface Antennas

Modeste Bodehou, Christophe Craeye, and Isabelle Huynen

Abstract—**A method based on the electric field integral equation is proposed for synthesizing planar metasurface (MTS) antennas built on elliptical apertures. The MTS is modeled with a modulated tensorial surface impedance. Entire-domain basis functions are used to discretize efficiently the currents as well as the surface impedance, allowing a quasi-direct computation of the surface impedance from the desired radiation pattern. The corresponding surface currents are combined with the near-field radiation from a constant reactance to derive the surface impedance of the MTS. The obtained algorithm is, therefore, systematic and can be applied to generate arbitrary radiation patterns, with control on the amplitude, phase, and polarization. Numerical validation of the proposed technique illustrates the effectiveness of the method.**

Index Terms—**Beam shaping, impedance boundary condition (IBC), integral equations (IE), modulated metasurface (MTS) antennas.**

I. Introduction

A formalism based on surface integral equations (IEs) has recently been used to design modulated metasurface (MTS) antennas on circular domains [1]. Depending on the type of radiation pattern and/or the azimuthal asymmetry of the feed, it may be more convenient to design the MTS on an elliptical aperture [2]. Indeed, in some practical cases, the radiated power density on the MTS is not azimutally symmetrical. Using an elliptical aperture, one can reduce the antenna footprint without significantly affecting the radiation pattern, and thus improve the antenna aperture efficiency [2]. This communication extends the synthesis algorithm proposed in [1] to elliptical domains.

Planar modulated MTS antennas are a class of leaky-wave antennas usually consisting of dense printed patches on a grounded substrate. The patches' layer implements a presynthesized sheet transition impedance boundary condition (IBC), which linearly relates the averaged tangential electric field to the averaged surface current on the MTS [3]–[5]. The radiation results from the modulation of the IBC through a perturbation of the surface wave (SW) generated by the antenna feed. This idea has been first highlighted in [6]. Since then, many authors have presented techniques for designing the surface impedance in order to control the antenna radiation pattern. The proposed methods were first based on holographic techniques [7] and have allowed the control of the aperture electric field phase [8], [9]. Then, Maci *et al.* [10] proposed for the first time an amplitude- and phase-based synthesis of the aperture field, which significantly widens the class of synthesizable aperture fields. Subsequently, Minatti *et al.* [11] proposed a flat optics-based iterative algorithm for synthesizing a class of radiating aperture electric fields. The used technique consists of locally expanding the fields on the aperture into Floquet harmonics. The surface impedance is then obtained after matching the desired radiating aperture field with the -1 mode of the Floquet expansion. A variant of the technique used in [11] has also been proposed in [12]. Once the surface impedance has been computed, the validation is usually carried out by solving the electric field IE (EFIE) with the method of moments (MoM) [13]–[16].

Manuscript received July 11, 2018; revised October 15, 2018; accepted October 19, 2018. Date of publication November 9, 2018; date of current version February 5, 2019. This work was supported by the Belgium Fonds National de la Recherche Scientifique Fund through the Fonds pour la formation à la recherche dans l'Industrie et dans l'Agriculture Grant. *(Corresponding author: Modeste Bodehou.)*

The authors are with the ICTEAM Institute, Université catholique de Louvain, 1348 Louvain-la-Neuve, Belgium (e-mail: modeste.bodehou@uclouvain.be; christophe.craeye@uclouvain.be; isabelle.huynen@uclouvain.be).

Color versions of one or more of the figures in this communication are available online at http://ieeexplore.ieee.org.

Digital Object Identifier 10.1109/TAP.2018.2880122

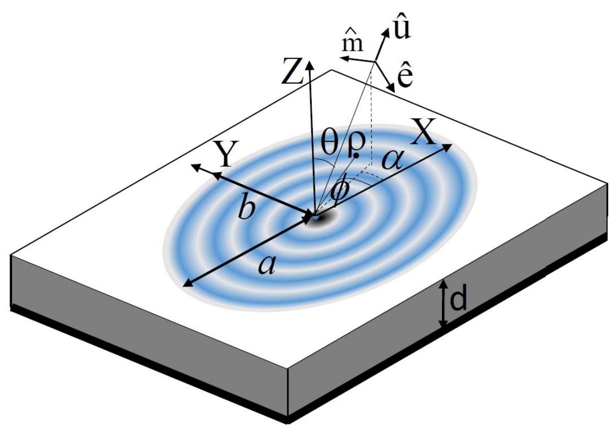

Fig. 1. Elliptical-domain modulated MTS antenna build with a grounded dielectric slab substrate.

Recently, Bodehou *et al.* [1] proposed a different synthesis approach directly based on the EFIE. This approach is no longer based on the local periodicity assumption but makes use of Fourier–Bessel basis functions (FBBFs, defined over the entire domain) to discretize efficiently the surface currents as well as the surface impedance. The EFIE is then inverted while constraining (in a least-squares sense) the surface impedance to be anti-Hermitian, as required for implementation with lossless patches. That results in a systematic and efficient algorithm able to generate arbitrary radiation patterns. This communication generalizes the procedure of [1] to the more general class of elliptical-domain MTSs. The latter have been analyzed using entire-domain basis functions in [16], where the ellipse is obtained from stretching the disk in one direction. It is shown in the following that this generalization does not significantly affect the computational complexity of the synthesis procedure.

The remainder of this communication is structured as follows. Section II presents the FBBFs, and the surface impedance and currents discretization. Section III describes the synthesis technique. Section IV provides a numerical validation of a designed surface impedance. Finally, Section V concludes this communication.

II. Currents and Surface Impedance Discretization

The MTS antennas of interest are realized on an elliptical aperture on the top ($z = 0$) of a grounded substrate [see Fig. 1]. The semimajor axis of the ellipse of length a is assumed without loss of generality to be along the $\hat{\boldsymbol{x}}$-axis and the semiminor axis of length b along the $\hat{\boldsymbol{y}}$-axis, where $\hat{\boldsymbol{x}}$ and $\hat{\boldsymbol{y}}$ are the unit vectors along the x- and y-directions, respectively. The vector $\boldsymbol{\rho} = (\rho, \phi)$ identifies an observation point on the MTS, where ρ and ϕ are, respectively, the radial and azimuthal coordinates. In such a structure, the FBBFs are defined as [16]

$$R_{m,n}(x, y) = F_{m,n}(\rho')e^{-jn\phi'} \tag{1}$$

where

$$F_{m,n}(\rho') = J_n\left(\lambda_n^m \rho'\right) \tag{2}$$

and $\rho' = \sqrt{(x/a)^2 + (yp/a)^2}$, $\tan(\phi') = yp/x$, $p = a/b > 1$, and λ_n^m is the mth positive zero of the Bessel function of order n. In this way, the (nonprimed) coordinates are defined over the ellipse, while the primed ones are defined over the corresponding disk. Those basis functions admit a closed-form Fourier transform $\tilde{R}_{m,n}(k_x, k_y)$ (see the Appendix), where k_x and k_y are the spectral variables in Cartesian coordinates. The surface current distribution is projected into its x- and y-components. Each component is then expanded into FBBFs as follows:

$$\mathbf{J}(x, y) = \sum_{n=-N}^{N} \sum_{m=1}^{M} i_{mn}^x R_{m,n}^x(x, y)\hat{\boldsymbol{x}} + i_{mn}^y R_{m,n}^y(x, y)\hat{\boldsymbol{y}}. \tag{3}$$

Note that contrary to [1] where a $(\hat{\boldsymbol{\rho}}, \hat{\boldsymbol{\phi}})$ polar representation was used for the vector and tensor expansions, we use here a $(\hat{\boldsymbol{x}}, \hat{\boldsymbol{y}})$ formulation. Indeed, in a polar system of coordinates, the unit vectors are no longer orthogonal after stretching the FBBFs. In this context, it has been found necessary to use the Cartesian reference system when dealing with an elliptical domain. For a circular domain, the $(\hat{\boldsymbol{\rho}}, \hat{\boldsymbol{\phi}})$ formulation is preferred, especially for a scalar IBC where the current is only directed along $\hat{\boldsymbol{\rho}}$.

Let us now assume that one is interested in synthesizing a capacitive tensorial sheet impedance of the form

$$\begin{aligned}
Z_S^{\rho\rho}(x, y) &= Z_0^{\rho\rho} + P^{\rho\rho}(x, y)\\
Z_S^{\rho\phi}(x, y) &= Z_S^{\phi\rho}(x, y) = P^{\rho\phi}(x, y)\\
Z_S^{\phi\phi}(x, y) &= Z_0^{\phi\phi} - P^{\rho\rho}(x, y)
\end{aligned} \tag{4}$$

where $\underline{\underline{\mathbf{Z}}}_0 = \mathrm{diag}(Z_0^{\rho\rho}, Z_0^{\phi\phi})$ is the unmodulated (average) reactance tensor and is assumed to be purely imaginary, with a negative imaginary part. Note that $Z_0^{\rho\rho}$ and $Z_0^{\phi\phi}$ do not need to be constant over the aperture. One can choose a given aperture variation according to the type of patches used for the IBC implementation. The only requirement is that they have to be known. The modulation functions $P^{\rho\rho}(x, y)$ and $P^{\rho\phi}(x, y)$ are also assumed to be purely imaginary. Finally, the modulation depth of each element of the tensor reactance ($m = \max|P|/|Z_0|$) is assumed to be smaller than 1. The above-mentioned capacitive tensorial sheet transition boundary condition is anti-Hermitian, as required to allow implementation with lossless patches [3]–[5]. The reactance tensor (4) written in a Cartesian system of coordinates then takes the following form:

$$\begin{aligned}
Z_S^{xx}(x, y) &= Z_0^{xx}(x, y) + P^{xx}(x, y)\\
Z_S^{xy}(x, y) &= Z_S^{yx}(x, y) = P^{xy}(x, y)\\
Z_S^{yy}(x, y) &= Z_0^{yy}(x, y) - P^{xx}(x, y)
\end{aligned} \tag{5}$$

where $Z_0^{xx}(x, y) = Z_0^{\rho\rho} - (Z_0^{\rho\rho} - Z_0^{\phi\phi})\sin^2\phi$ and $Z_0^{yy}(x, y) = Z_0^{\rho\rho} - (Z_0^{\rho\rho} - Z_0^{\phi\phi})\cos^2\phi$ are the average reactances in the Cartesian system of coordinates. The IBC (5) is then discretized into FBBFs as follows:

$$Z_S^{xx} \approx \sum_{n_S, m_S} \left[K_S^{xx}(m_S, n_S) + X_S^{xx}(m_S, n_S)\right] R_{m_S, n_S} \tag{6}$$

$$Z_S^{xy} \approx \sum_{n_S, m_S} X_S^{xy}(m_S, n_S) R_{m_S, n_S} \tag{7}$$

$$Z_S^{yy} \approx \sum_{n_S, m_S} \left[K_S^{yy}(m_S, n_S) - X_S^{xx}(m_S, n_S)\right] R_{m_S, n_S} \tag{8}$$

where the (x, y) dependence has been implicitly omitted and $K_S^{xx}(m_S, n_S)$ and $K_S^{yy}(m_S, n_S)$ correspond, respectively, to the expansion coefficients of the average reactances Z_0^{xx} and Z_0^{yy} into FBBFs. Since FBBFs are orthogonal, this expansion is carried out through a simple projection.

A spatial FBBF decomposition of a function $f(x, y)$ can be obtained as

$$a_{mn} = \frac{p}{K_0(m, n)} \iint f(x, y) R_{m,n}^*(x, y) dx\, dy \tag{9}$$

where $K_0(m, n) = -\pi a^2 J_{n-1}(\lambda_{nm}) J_{n+1}(\lambda_{nm})$ and the integration is carried out over the elliptical domain. The superscript (*) corresponds to the complex conjugate. To evaluate this integral, it is more convenient to stretch the ellipse into the circle through the change of variables $x' = x$ and $y' = yp$. One obtains

$$a_{mn} = \frac{1}{K_0(m, n)} \iint f\left(x', \frac{y'}{p}\right) R_{m,n}^*\left(x', \frac{y'}{p}\right) dx' dy'. \tag{10}$$

The function $R_{m,n}(x', y'/p)$ corresponds to a circular-domain FBBF of radius a as defined in [15]. It means that projecting a function $f(x, y)$ over an elliptical-domain FBBF is equivalent to projecting the function $f(x, y/p)$ over the corresponding circular-domain FBBF. This operation is much less time consuming since the azimuthal integration can be done with the fast Fourier transform and the radial part with the Gauss–Legendre quadrature, as explained in [15].

The parameters $X_S^{xx}(m_S, n_S)$ and $X_S^{xy}(m_S, n_S)$ in (6)–(8) are the unknowns expansion coefficients of the surface impedance modulation. Since $P^{xx}(x, y)$ and $P^{xy}(x, y)$ are assumed to be purely imaginary, the coefficients $X_S^{xx}(m_S, n_S)$ and $X_S^{xy}(m_S, n_S)$ need to satisfy the following symmetry:

$$(X_S(m_S, -n_S))^* = -\frac{X_S(m_S, n_S)}{(-1)^n} \tag{11}$$

where we have omitted the superscripts xx and xy.

The synthesis problem then consists of finding the reactance modulation, which will provide the desired radiation pattern. In the remainder of this communication, basis functions with subscripts S, t, and b refer to decomposition of the surface impedance, fields, and currents, respectively.

III. Synthesis of the MTS

We first make the assumption that the substrate, the average sheet transition IBC $\underline{\underline{\mathbf{Z}}}_0$, and the MTS excitation are *a priori* known. The excitation is designed to maximize the power balance between the excited SW and the directly radiated space wave. The above-mentioned choices usually depend on other considerations relative to the feed efficiency, the IBC implementation process with patches, and the bandwidth. These issues are outside the scope of this communication and have been already treated in [18], [19].

Now, let us assume that one is interested in generating a given known radiation pattern $\mathbf{F}(\theta, \alpha)$ in amplitude, phase, and polarization, where $\mathbf{F}$ is the spatial electric field distribution in the far field, and θ and α are, respectively, the elevation and azimuthal angles [see Fig. 1]. We define the observation direction as

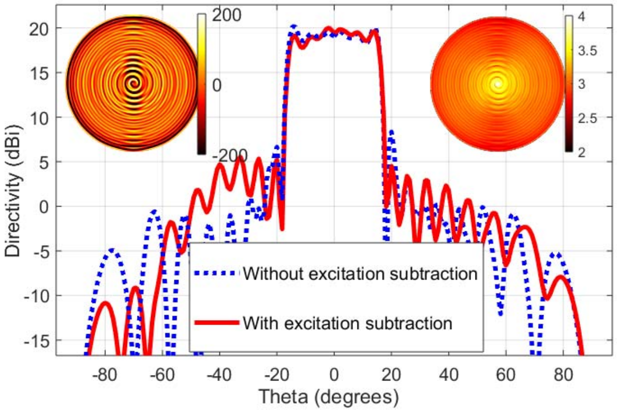

Fig. 2. Cut in the $\alpha = 0$ plane of the copolar radiation pattern. The result obtained after subtracting the aperture electric field generated by the feed is compared with that obtained without subtracting the feed contribution. The left and the right inset disks correspond, respectively, to the $\rho\rho$ component of the synthesized reactance (obtained without feed field subtraction), and the corresponding absolute value of the current distribution (in $\log_{10}$ scale).

$\hat{u} = (u_x, u_y, u_z) = (\sin\theta\cos\alpha, \sin\theta\sin\alpha, \cos\theta)$, and their corresponding spectral variables as $(k_x, k_y, k_z) = k_0\,\hat{u}$, where k_0 is the free-space wavenumber. The radiation pattern $\mathbf{F}$ is linked to the visible part spectrum of the tangential electric field $\tilde{\mathbf{f}}$ on the MTS as follows:

$$\begin{bmatrix} \tilde{f}_x \\ \tilde{f}_y \end{bmatrix} = \frac{-2\pi}{jk_0 u_z\sqrt{1-u_z^2}} \begin{bmatrix} u_y & -u_x u_z \\ -u_x & -u_y u_z \end{bmatrix} \begin{bmatrix} F_{TE} \\ F_{TM} \end{bmatrix} \tag{12}$$

where $\eta_0 \approx 377\Omega$ is the free-space impedance. F_{TE} and F_{TM} are the components of the radiation pattern $\mathbf{F}(\theta, \alpha)$, respectively, parallel to $\hat{m}$ and $\hat{e}$ vectors in Fig. 1. The visible spectrum corresponds to the part of the spectrum for which $\sqrt{k_x^2 + k_y^2} < k_0$. The corresponding visible current spectrum is then obtained as

$$\tilde{\mathbf{J}} = (\underline{\underline{\tilde{\mathbf{G}}}}^{EJ})^{-1}(\tilde{\mathbf{f}} - \tilde{\mathbf{E}}_i) \tag{13}$$

where $\underline{\underline{\tilde{\mathbf{G}}}}^{EJ}$ is the dyadic spectral Green's function of the grounded substrate [20], $\tilde{\mathbf{E}}_i$ is the visible spectrum of the MTS excitation, and $\tilde{\mathbf{f}}$ is rescaled with respect to the radiated power. The latter has been computed using the technique described in [1]. For the synthesized MTSs, we have observed that $\tilde{\mathbf{E}}_i$ can be neglected in comparison with $\tilde{\mathbf{f}}$. This assumption has been implicitly made in [1]. As an example, Fig. 2 compares the radiation pattern obtained in [1, Sec. V.B], where $\tilde{\mathbf{E}}_i$ has been neglected in the synthesis, with that obtained without neglecting $\tilde{\mathbf{E}}_i$, both for a circular-domain MTS. One can observe that a very similar performance has been achieved. When the visible part of $\tilde{\mathbf{E}}_i$ is much smaller than $\tilde{\mathbf{f}}$, it is difficult to say whether the subtraction in (13) will be favorable to the final design. This should be decided based on correspondence between final full-wave simulation and initially the desired radiation pattern.

At this moment, only the visible part of the current spectrum is known. To synthesize the MTS, one also needs the invisible (near-field) part. This near-field part cannot be neglected since the radiation phenomenon comes from the leakage of an SW. For some canonical patterns, analytical expressions of the near field have been proposed in [10]. However, when one is dealing with an arbitrary radiation pattern, finding the appropriate near-field part is not an easy task. Therefore, as in [1], we make in a first instance, the simplest assumption, i.e., the near-field spectrum is obtained in the absence of modulation. This is the simplest possible estimation since it does not even take into account the leakage rate $\alpha(x, y)$ nor the phase constant variation $\Delta\beta(x, y)$ on the MTS aperture. In passing, finding *a priori* these parameters for an arbitrary-shaped pattern is not a well-posed problem. This "simplest" invisible current spectrum, in combination with the visible spectrum part (obtained from the pattern), forms a first estimate of the current distribution spectrum $\tilde{\mathbf{J}}$ on the MTS. The corresponding surface impedance can then be obtained after solving the EFIE. Following the same reasoning as described in [1], one obtains that the IBC modulation satisfies the following equation:

$$\begin{bmatrix} \mathbf{X}_S^{xx} \\ \mathbf{X}_S^{xy} \end{bmatrix} \begin{bmatrix} \mathbf{Z}^{S,x} & \mathbf{Z}^{S,y} \\ -\mathbf{Z}^{S,y} & \mathbf{Z}^{S,x} \end{bmatrix} = \underline{\mathbf{U}} \tag{14}$$

where $\mathbf{X}_S^{xx}$ and $\mathbf{X}_S^{xy}$ are the expansion coefficients of the IBC modulation given in (6)–(8). $\mathbf{Z}^{S,x}$ and $\mathbf{Z}^{S,y}$ are defined as

$$Z^{S,x}(m_S, n_S; m_t, n_t) = \sum_{n_b, m_b} i^x_{m_b n_b} Z(m_b, n_b; m_S, n_S; m_t, n_t) \tag{15}$$

$$Z^{S,y}(m_S, n_S; m_t, n_t) = \sum_{n_b, m_b} i^y_{m_b n_b} Z(m_b, n_b; m_S, n_S; m_t, n_t) \tag{16}$$

with $\mathbf{Z} = (a^2/p)\mathbf{Z}_U$, where $\mathbf{Z}_U$ is tabulated and has been defined in [1], [15].

The vector $\underline{\mathbf{U}}$ is computed as

$$\underline{\mathbf{U}} = \begin{bmatrix} \mathbf{U}^x \\ \mathbf{U}^y \end{bmatrix} = \begin{bmatrix} \mathbf{Z}_G^{xx} & \mathbf{Z}_G^{xy} \\ \mathbf{Z}_G^{yx} & \mathbf{Z}_G^{yy} \end{bmatrix} \begin{bmatrix} \mathbf{I}^x \\ \mathbf{I}^y \end{bmatrix} - \begin{bmatrix} \mathbf{V}^x \\ \mathbf{V}^y \end{bmatrix} - \begin{bmatrix} \mathbf{X}_K^x \\ \mathbf{X}_K^y \end{bmatrix} \tag{17}$$

where $\mathbf{Z}_G^{xx}$, $\mathbf{Z}_G^{xy}$, $\mathbf{Z}_G^{yx}$, and $\mathbf{Z}_G^{yy}$ are the different components of the substrate interaction matrix. They can be computed using the procedure described in [16]. $\mathbf{I}^x$ and $\mathbf{I}^y$ are the column vectors with the expansion coefficients (into FBBFs) of the previously estimated surface current distribution $\tilde{\mathbf{J}}$, along $\hat{a}_x$ and $\hat{a}_y$, respectively. Those expansion coefficients are computed through a spectral-domain projection of $\tilde{\mathbf{J}}$ (20). $\mathbf{V}^x$ and $\mathbf{V}^y$ correspond to the excitation vector. They are computed in the same way as in [16]. Finally, $\mathbf{X}_K^x$ and $\mathbf{X}_K^y$ are defined as

$$\mathbf{X}_K^x = \mathbf{Z}^{S,x}\mathbf{K}_S^{xx} \tag{18}$$

$$\mathbf{X}_K^y = \mathbf{Z}^{S,y}\mathbf{K}_S^{yy} \tag{19}$$

where $\mathbf{K}_S^{xx}$, and $\mathbf{K}_S^{yy}$ are the vectors, respectively, containing the expansion coefficients of the known average reactance Z_0^{xx} and Z_0^{yy}. The excitation vectors $\mathbf{V}^x$ and $\mathbf{V}^y$ correspond to the projections of the excitation fields on the entire-domain testing functions. As such, they can be computed for elementary dipole as well as for more realistic extended feeding structures. Equation (14) is solved while imposing the symmetry (11) in the coefficients of $\mathbf{X}_S^{xx}$ and those of $\mathbf{X}_S^{xy}$ in order to constrain the impedance to be anti-Hermitian. This condition is imposed in the least-squares sense (see [1, Sec. IV.A]), which in turn leads to significant changes in the current distribution, including in its invisible (i.e., nonradiating) part. The surface currents and far fields are then simulated with the MoM using the derived anti-Hermitian IBC. Depending on the obtained modulation depth or the generated pattern performance, the radiated power is tuned accordingly.

The resulting algorithm is then the same as in [1], except that the EFIE operator is given by (14), the spatial projection operation is given by (10), and the spectral projection of a function $\tilde{f}(k_x, k_y)$ over an elliptical-domain FBBF spectrum is equivalent to projecting the function $p\tilde{f}(k_x, k_y p)$ over the following circular-domain FBBF spectrum:

$$\frac{1}{\tilde{K}_0(m,n)} \iint p\tilde{f}(k'_x, k'_y p)\tilde{R}^*_{m,n}(k'_x, k'_y p)dk'_x dk'_y \tag{20}$$

where $\tilde{K}_0(m,n) = -4\pi^3 a^2 J_{n-1}(\lambda_{nm})J_{n+1}(\lambda_{nm})$. This leads to an MTS synthesis process over an elliptical domain that is almost as

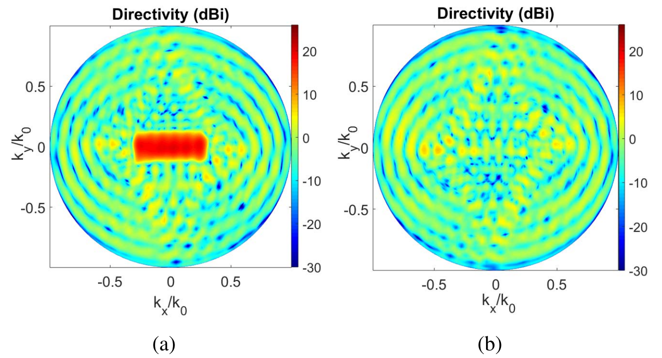

Fig. 3. Circularly polarized radiation pattern in the spectral (k_x, k_y) plane. (a) Copolar component for designed MTS. (b) Cross-polar component for designed MTS.

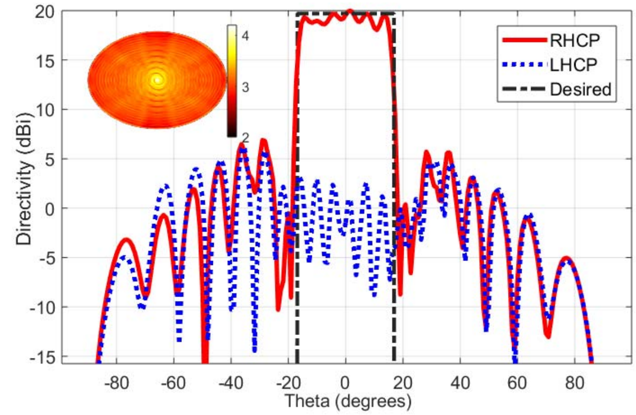

Fig. 4. Cut in the $\alpha = 0$ plane of the radiation pattern for the designed rectangular beam radiating MTS. The right-handed circular polarization (RHCP) and the left-handed circular polarization (LHCP), respectively, correspond to the copolar and cross-polar directivities. Inset disk: absolute value of the current distribution on the designed MTS (in $\log_{10}$ scale) for a unit current excitation.

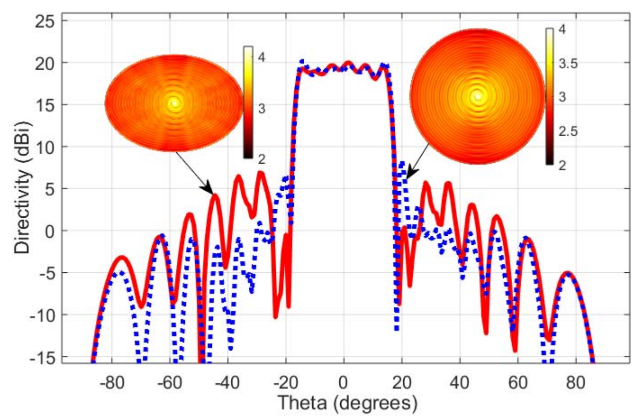

Fig. 5. Cut in the $\alpha = 0$ plane of the copolar radiation pattern. The result obtained with the designed elliptical-domain MTS is compared with that of the circular-domain MTS. Inset disks: absolute value of the current distribution (in $\log_{10}$ scale) on the elliptical MTS and on the circular MTS for a unit current excitation.

fast as that for a circular domain, when using the same number of basis functions for sheet impedance and currents. The only difference resides in the computation of the substrate matrix interaction $\underline{\underline{\mathbf{Z}}}_G$, which requires for elliptical domain, a harmonic development of the Green's function [16]. However, this matrix needs to be computed only once for any pattern once the aperture size and the substrate are known since $\underline{\underline{\mathbf{Z}}}_G$ does not depend on the IBC.

IV. Numerical Validation

This section presents a numerical validation (based on the MoM algorithm validated in [16], [17]) of a synthesized elliptical-domain MTS IBC. The MTS has been designed to radiate a spectral circularly polarized rectangular beam and is fed with a vertical elementary dipole placed at the center ($\rho = 0$), and in the middle of the grounded substrate ($z = -d/2$), where d is the substrate thickness [see Fig. 1]. This beam is defined as $F_{TE} = \cos\alpha - j\sin\alpha$ and $F_{TM} = \sin\alpha + j\cos\alpha$ for $-\Delta k_x < k_x < \Delta k_x$, $-\Delta k_y < k_y < \Delta k_y$ and $F_{TE} = F_{TM} = 0$ elsewhere. TE and TM stand, respectively, for the transverse electric and transverse magnetic components of the electric far field $\mathbf{F}$. We have chosen $\Delta k_x = 0.29\ k_0$ and $\Delta k_y = 0.09\ k_0$. This beam has already been designed in [1, Sec. V.B] considering a circular domain. As can be seen from the results presented in [1, Sec. V.B], the surface current distribution is azimuthally no symmetrical since the modulation depth is larger in the y-direction than in the x-direction. This is consistent with the pattern shape. For such a pattern, one can reduce the size of the disk in the y-direction without significantly affecting the radiation performance. However, simply cutting the MTS will not lead to optimal performance since the radiation originates from a global effect. In this communication, we designed the MTS on an ellipse with semimajor axis equal to the radius used in [1], i.e., 10λ and a semiminor axis equal to 7λ, thus leading to $p \approx 1.429$. The operating frequency is 18 GHz and the substrate parameters are the same as in [1]. The design has been carried out using the following values defining the number of basis functions $N_S = 20$, $M_S = 50$, $N_b = N_t = 20$, $M_b = M_t = 55$, and the designed MTS IBC has been analyzed with the method presented in [16], using $N_b = N_t = 30$ and $M_b = M_t = 60$, which leads to 7320 basis functions. Fig. 3 shows the obtained radiation pattern in the spectral (k_x, k_y) plane, and Fig. 4 represents a cut of this pattern in the $\alpha = 0$ plane. Fig. 5 compares the computed copolar radiation pattern with that obtained in [1, Sec. V-B], corresponding to a circular-domain MTS of radius equal to the semimajor axis of the ellipse.

One can see that almost the same gain has been achieved compared to [1, Sec. V.B], but using only 70% of the initial surface.

TABLE I
Computation Times for the Designed IBC

Solver	Circular domain	Elliptical domain
Substrate matrix	15 s	5.3 min
Invisible spectrum	46 s	52 s
Radiated power	1.1 min	1.1 min
Visible spectrum	2.3 min	2.4 min
EFIE inversion	3.7 min	8.2 min
Total computation time	8.1 min	17.86 min

Finally, the synthesis computation time is summarized in Table I, where a comparison between the circular-domain synthesis and the elliptical-domain synthesis is also made. The code has been developed using the MATLAB language [21] on a conventional laptop computer.

One can observe that the main difference when going from circular domain to elliptical domain is related to the substrate matrix computation, which requires a harmonic development of Green's function. It is worth mentioning that this matrix has to be computed only once in an optimization procedure since it does not depend on the surface impedance nor on the excitation. However, the overall computation time is dominated by the solution of the EFIE (including matrix filling) in the least-squares sense, which allows the derivation of the reactance from the objective currents. In this example, the latter operation is more time consuming for the elliptical domain due to the finer azimuthal discretization required (N = 20 versus N = 15).

V. Conclusion

We have presented an extension of the work in [1], which proposed a systematic IE-based design of circular-domain MTS antennas. The illustrative example shows that the antenna aperture efficiency can be significantly improved using an elliptical domain, as compared to the case of the classical circular aperture. Although orthogonal entire-domain basis functions have been used here, these properties are not mandatory, i.e., the method can be adapted for local, nonorthogonal basis functions. However, in those cases, the projection operations need to be carried out by solving a linear system of equations, which is much more time and memory consuming. Local basis functions have advantages of coping with arbitrary shapes. However, discretizing typical current distributions on MTSs with such a basis requires typically more than 50 000 unknowns [14], for which direct inversion is unfeasible on classical personal computers.

Appendix
FBBF Fourier Transform

The Fourier transform of the FBBFs, as defined in (1), is given as

$$\tilde{R}_{m,n}(k_x,k_y) = -\frac{2\pi j^n e^{-jn\alpha'}}{p}\left[\frac{a^2\lambda_n^m J_{n-1}(\lambda_n^m)J_n(k'_\rho a)}{(\lambda_n^m)^2-(k'_\rho a)^2}\right] \quad (21)$$

where $k'_\rho = \sqrt{(k_x)^2+(k_y/p)^2}$, $\tan(\alpha') = k_y/(pk_x)$, and k_x and k_y are the spectral variables written in a Cartesian system of coordinates.

References

[1] M. Bodehou, C. Craeye, E. Martini, and I. Huynen, "A Quasi-direct method for the surface impedance design of modulated metasurface antennas," *IEEE Trans. Antennas Propag.*, to be published.

[2] M. Casaletti, M. Śmierzchalski, M. Ettorre, R. Sauleau, and N. Capet, "Polarized beams using scalar metasurfaces," *IEEE Trans. Antennas Propag.*, vol. 64, no. 8, pp. 3391–3400, Aug. 2016.

[3] E. Martini, M. Mencagli, Jr., and S. Maci, "Metasurface transformation for surface wave control," *Philos. Trans. Roy. Soc. London A, Math. Phys. Sci.*, vol. 373, no. 2049, pp. 2992–3003, Jul. 2015.

[4] A. M. Patel and A. Grbic, "Modeling and analysis of printed-circuit tensor impedance surfaces," *IEEE Trans. Antennas Propag.*, vol. 61, no. 1, pp. 211–220, Jan. 2013.

[5] A. M. Patel and A. Grbic, "Effective surface impedance of a printed-circuit tensor impedance surface (PCTIS)," *IEEE Trans. Microw. Theory Techn.*, vol. 61, no. 4, pp. 1403–1413, Apr. 2013.

[6] A. A. Oliner and A. Hessel, "Guided waves on sinusoidally-modulated reactance surfaces," *IRE Trans. Antennas Propag.*, vol. 7, no. 5, pp. 201–208, Dec. 1959.

[7] B. H. Fong, J. S. Colburn, J. J. Ottusch, J. L. Visher, and D. F. Sievenpiper, "Scalar and tensor holographic artificial impedance surfaces," *IEEE Trans. Antennas Propag.*, vol. 58, no. 10, pp. 3212–3221, Oct. 2010.

[8] G. Minatti, S. Maci, P. De Vita, A. Freni, and M. Sabbadini, "A circularly-polarized isoflux antenna based on anisotropic metasurface," *IEEE Trans. Antennas Propag.*, vol. 60, no. 11, pp. 4998–5009, Nov. 2012.

[9] S. Maci, G. Minatti, M. Casaletti, and M. Bosiljevac, "Metasurfing: Addressing waves on impenetrable metasurfaces," *IEEE Antennas Wireless Propag. Lett.*, vol. 10, pp. 1499–1502, 2011.

[10] G. Minatti *et al.*, "Modulated metasurface antennas for space: Synthesis, analysis and realizations," *IEEE Trans. Antennas Propag.*, vol. 63, no. 4, pp. 1288–1300, Apr. 2014.

[11] G. Minatti, F. Caminita, E. Martini, M. Sabbadini, and S. Maci, "Synthesis of modulated-metasurface antennas with amplitude, phase, and polarization control," *IEEE Trans. Antennas Propag.*, vol. 64, no. 9, pp. 3907–3919, Sep. 2016.

[12] M. Teniou, H. Roussel, N. Capet, G.-P. Piau, and M. Casaletti, "Implementation of radiating aperture field distribution using tensorial metasurfaces," *IEEE Trans. Antennas Propag.*, vol. 65, no. 11, pp. 5895–5907, Nov. 2017.

[13] M. A. Francavilla, E. Martini, S. Maci, and G. Vecchi, "On the numerical simulation of metasurfaces with impedance boundary condition integral equations," *IEEE Trans. Antennas Propag.*, vol. 63, no. 5, pp. 2153–2161, May 2015.

[14] D. González-Ovejero and S. Maci, "Gaussian ring basis functions for the analysis of modulated metasurface antennas," *IEEE Trans. Antennas Propag.*, vol. 63, no. 9, pp. 3982–3993, Sep. 2015.

[15] M. Bodehou, D. González-Ovejero, C. Craeye, and I. Huynen, "Method of Moments simulation of modulated metasurface antennas with a set of orthogonal entire-domain basis functions," *IEEE Trans. Antennas Propag.*, to be published.

[16] M. Bodehou, C. Craeye, H. Bui-Van, and I. Huynen, "Fourier–Bessel basis functions for the analysis of elliptical domain metasurface antennas," *IEEE Antennas Wireless Propag. Lett.*, vol. 17, no. 4, pp. 675–678, Apr. 2018.

[17] M. Bodehou, S. Hubert, H. A. Kayani, C. Craeye, and I. Huynen, "Analysis of elliptical aperture metasurface antennas," in *Proc. 12th Int. Congr. Artif. Mater. Novel Wave Phenomena.*, Aug. 2018.

[18] G. Minatti, E. Martini, and S. Maci, "Efficiency of metasurface antennas," *IEEE Trans. Antennas Propag.*, vol. 65, no. 4, pp. 1532–1541, Apr. 2017.

[19] G. Minatti, M. Faenzi, M. Sabbadini, and S. Maci, "Bandwidth of gain in metasurface antennas," *IEEE Trans. Antennas Propag.*, vol. 65, no. 6, pp. 2836–2842, Jun. 2017.

[20] L. Vegni, R. Cicchetti, and P. Capece, "Spectral dyadic Green's function formulation for planar integrated structures," *IEEE Trans. Antennas Propag.*, vol. 36, no. 8, pp. 1057–1065, Aug. 1998.

[21] *MATLAB R2015a*, MathWorks, Inc., Natick, MA, USA, 2015.